CCS Chemistry

RESEARCH ARTICLE

Received: Dec. 8, 2025 | Accepted: Feb. 4, 2026 | Published: Mar. 13, 2026

Elucidating the Sodium Insertion Mechanism of an Organic Electrode Material for Sodium-Ion Batteries

Maximillian G. Stanzione[1], Oxana V. Magdysyuk[1], Daniel J. M. Irving[2], Chinnasamy Murugesan[1,3], Nicole L. Kelly[1], Yingling Liao[1,3], Pech Thongkam[1,3], Heitor S. Seleghini[1], Paul S. Wheatley[1], David B. Cordes[1], Simon J. Coles[4], Daniel N. Rainer[4], Aamod V. Desai[1,3,5], Sharon E. Ashbrook[1], Julia L. Payne[1], Russell E. Morris[1,3] & A. Robert Armstrong[1,3]*

[1]EaStCHEM School of Chemistry, St Andrews KY16 9ST, [2]Diamond Light Source Ltd, Didcot OX11 0D3, [3]The Faraday Institution, Didcot OX11 0RA, [4]School of Chemistry and Chemical Engineering, University of Southampton, Southampton SO17 1BJ, [5]Department of Chemistry, Indian Institute of Technology Madras, Chennai 600036

Corresponding author: ARA@st-andrews.ac.uk

Cite this: *CCS Chem*. **2026**, Just Published. DOI: 10.31635/ccschem.026.202507155

Organic anode materials for sodium-ion batteries are attracting a great deal of interest due to their sustainability and design flexibility. However, the Na^+ insertion mechanism is poorly understood, especially for disordered organic anode materials. A lack of understanding restricts optimization efforts and potential commercialization. Herein, we apply a range of characterization techniques, such as three-dimensional electron diffraction, powder X-ray diffraction, Raman spectroscopy, electron paramagnetic resonance spectroscopy, and pair distribution function (PDF) analysis to a model system, sodium naphthalene-2,6-dicarboxylate, to elucidate the Na^+ storage mechanism. A combined ab initio random structure search and PDF study was conducted to postulate a structure of sodiated Na_{2+x}NDC (s-NDC). Our work reveals an expansion in the Na^+–O storage layer to allow for the accommodation of inserted Na^+. Meanwhile, the naphthalene units exist as radical species, promoting a reorientation to accommodate the inserted Na^+, as well as facilitating a stabilizing π interaction. Ultimately, our results illustrate the efficacy of using a multi-technique approach to study the sodiation mechanism of an organic anode material and offer insight into the sodiated structure. This approach can inform the strategic molecular design of future organic anode materials.

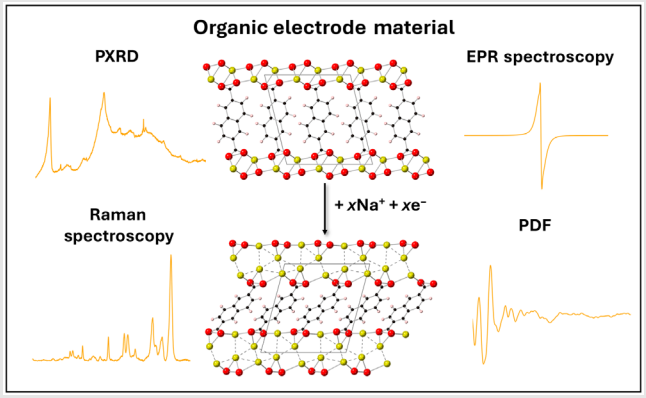

Keywords: pair distribution function, organic electrodes, chemical structure, chemical sodiation, Raman spectroscopy, sodium-ion batteries

Introduction

Sodium-ion batteries are already a commercial reality and are beginning to capture some of the energy storage market. Curtailing sodium-ion batteries from taking a wider share of the energy storage market is the lack of a suitable anode material. Among the variety of possible materials tipped to be suitable candidates are organic materials. They are sustainable, inexpensive, and with recent advances in green synthesis offer unique

Citation: *CCS Chem*. **2026**, Just Published. DOI: 10.31635/ccschem.026.202507155
Link to VoR: https://doi.org/10.31635/ccschem.026.202507155

advantages over their competitors.[1-4] However, research into the mechanism of Na^+ insertion is still in its nascency. Understanding how a material behaves as an electrode is critical to future design strategies and developing informed optimization approaches for current candidates. Organic electrode material is a broad term that can encompass materials from polymers to Schiff bases.[5] Specifically, small molecule organic electrodes such as sodium based organic carboxylates are an intriguing class of material because of their sustainability, their respectable capacities, and ease of synthesis.[2-4,6] Studying how organic electrode materials work can be incredibly challenging due to the weak scattering of X-rays and the amorphization that often occurs upon discharge and charge. The additional components (carbon-based conductive additives) in the electrode further complicate matters, often being of similar scattering power to the active electrode material. This results in lower signal to noise, and makes signal separation complex for X-ray-based techniques, therefore making analysis difficult. There are a few examples of organics retaining crystallinity upon discharge.[7] Wu et al.[7] conducted a study that consisted of a direct space approach using combined computational and experimental techniques, including in situ powder X-ray diffraction (PXRD) data, and geometry optimization using density functional theory (DFT). This allowed Wu et al.[7] to postulate a sodiation mechanism. However, relying on crystalline organic materials restricts studying the wider field of organic materials that do not retain crystallinity upon Na^+ insertion. Evidently, further work using nontraditional characterization techniques is required to enable the study of the Na^+ insertion mechanism in such materials. Due to the increase in disorder that often occurs upon Na^+ insertion, a technique without a prerequisite for long-range order is required. One suitable technique is pair distribution function (PDF) analysis using total scattering data. This technique has been widely applied to other classes of anode materials, including in the study of alloying materials and hard carbons, where it has been used for revealing sodiation mechanisms in an energy storage context.[8-10] However, complications due to the presence of binder and conductive additives still remain, as similar scattering can confuse the signal contribution. One possible solution is chemical sodiation to synthesize a "model" sodiated structure, which can then be referenced to what is produced electrochemically. Chemical sodiation has been widely used in the context of presodiation, a methodology designed to pretreat the electrode material to improve the electrochemical performance.[11-13] There is a range of sodium-based reducing agents suitable for use on organic electrode materials. A well-established group of organic electrodes are sodium carboxylates, with benzene, naphthalene, and anthracene derivatives all previously studied for their electrochemical performance.[14-16] The dicarboxylate compound, sodium naphthalene-2,6-dicarboxylate (Na_2NDC), has previously demonstrated impressive rate performance in sodium half-cells alongside respectable gravimetric capacity, placing it as an attractive choice of organic anode; the amorphization of Na_2NDC upon Na^+ insertion has also previously been shown.[15,17] The theoretical Na^+ insertion mechanism of Na_2NDC is a 2-electron, 2 Na^+ insertion to produce Na_4NDC as postulated by Deng et al.[18] and Cabañero Jr et al.[15] but the mechanism of Na^+ insertion is still poorly understood, due to the difficulties in characterizing the disordered structure after Na^+ insertion.[15,17] Herein, we employed a combined computational and experimental approach to understand the Na^+ insertion mechanism of Na_2NDC. By utilizing a range of characterization techniques such as PDF, we studied how Na_2NDC can store Na^+. We investigated the structural and electronic transformations that accompany Na^+ insertion. A chemical sodiation procedure was used to enable investigation of the Na^+-inserted $Na_{2+x}NDC$ (s-NDC) structure without interference from the conductive additive or binder. Ex situ PDF data of s-NDC at different degrees of chemical sodiation and at different states of electrochemical sodiation were collected. A computational ab initio random structure search (AIRSS) study generated a series of candidate sodiated structures, which subsequently underwent geometry optimization using DFT.[19,20] Three candidate structures then underwent a simulated annealing and real-space least-squares refinement procedure against the PDF data of the chemically sodiated s-NDC. One candidate structure was selected for further study based on its agreement to the experimental data. The candidate structure subsequently underwent the same simulated annealing and real-space least-squares refinement procedure in a reduced symmetry space group (*P*1). A final simulated annealing and real-space least-squares refinement was completed in a 1x3x1 supercell to elucidate the structural changes that occur due to sodiation. Importantly, the calculated PXRD pattern of the structure postulated using PDF, a local structural probe, closely matched the ex situ PXRD data. Supporting this work, three-dimensional electron diffraction (3D ED) provided the first single crystal structure solution of the Na_2NDC structure. Differential PDF (dPDF) and operando Raman spectroscopy were used to confirm the consistency between the chemical and electrochemical Na^+ insertion products. Ex situ electron paramagnetic resonance (EPR) techniques were used to probe the redox mechanism and the electronic changes that occur upon redox. The combined approach offered insight into the average Na^+ co-ordination environment and the reorientation of the organic unit upon redox. This strategy outlines a methodology that can be used to elucidate how disordered organic electrode materials function and can inform future design strategies to create superior organic electrode materials.

Citation: *CCS Chem.* **2026**, Just Published. DOI: 10.31635/ccschem.026.202507155
Link to VoR: https://doi.org/10.31635/ccschem.026.202507155

Experimental Methods

Na_2NDC was synthesized according to the method of Cabañero Jr et al.[15] by pre-dissolving sodium hydroxide (Pellets, Fisher Scientific, United Kingdom) in methanol (Anhydrous, ca. 100 mL, Sigma Aldrich, United Kingdom). After dissolution, naphthalene-2,6-dicarboxylic acid (99%, Sigma Aldrich) was added to the solution while stirring at room temperature. A white precipitate formed within 20 min. The suspension was then stirred at 80 °C under reflux for 24 h. The hot solution was vacuum filtered and washed with methanol (ca. 30 mL). The resulting powder was then dried overnight in an oven at 80 °C.

1 M and 0.5 M sodium biphenyl (NaBP) solutions were prepared. The correct amount of biphenyl (99.5%, Sigma Aldrich, United Kingdom) was weighed out and added to 5 mL of 1,2-dimethoxyethane (DME, anhydrous, 99.5%, inhibitor-free, Sigma Aldrich) while stirring and allowed to dissolve. Subsequently, the correct amount of sodium metal (99.9%, trace metal basis, Sigma Aldrich) was added to the solution. The sodium metal immediately dissolved to produce a dark blue hue. The NaBP was subsequently always kept in an argon atmosphere. The solution was left to stir overnight before use as a reducing agent. All DME was stored over 4 Å molecular sieves for a minimum of 10 days to ensure that no residual water was present.

To synthesize chemically sodiated Na_2NDC, approximately 50 mg of the polycrystalline powder was dried at 80 °C and then ground with a pestle and mortar and transferred to a beaker. A stoichiometric amount of NaBP in DME was added. The reaction was left for 1 min. After 1 min, the reaction mixture was washed with DME (4 mL) to quench the reaction. After washing, with DME, the suspension was left to settle for 5 min. The DME biphenyl solution was then pipetted out, leaving the brown/black powder as the product (s-NDC). The remaining brown/black powder was then left to dry in the glovebox and dried under vacuum overnight. The s-NDC product was subsequently always kept in an argon atmosphere.

Na_2NDC electrodes were prepared by combining 70 wt % active material with 30 wt % super C65 carbon (Imerys, France). The electrode was then dried under vacuum overnight at 80 °C before use. For electrochemical testing, CR2032 coin cells and Swagelok cells were used. CR2032 coin cells were used for EPR and PDF experiments. Swagelok cells were used for PXRD experiments. All cells were prepared in an argon-filled glovebox. Metallic sodium was used as the counter electrode. Two separators were used, a Whatman GF/F glass fibre separator and a Cellgard separator, soaked in electrolyte for CR2032 coin cells. Three Whatman GF/F glass fiber separators were used for Swagelok cells. The electrolyte system was 1 M $NaPF_6$ in ethylene carbonate/diethyl carbonate (1:1 v/v, E-Lyte, Germany). Cells were cycled in galvanostatic mode on a Neware BTS4000-5V10mA battery testing system (Neware, Shenzhen, China) at 30 °C at 10 mA g^{-1}. The reference carbon electrode was 100 wt % super C65 (Imerys) was fabricated in a CR2032 coin cell analogous to the Na_2NDC electrodes.

To obtain ex situ samples, cycled cells were placed in an argon-filled glovebox, deconstructed, and the active electrode was washed with dimethyl carbonate (DMC, anhydrous >99%, Sigma Aldrich, United Kingdom) for at least 30 min. After washing, the DMC was removed, and the electrode mixture was dried overnight under vacuum. The sample was then loaded into capillaries and sealed.

All PXRD patterns were measured at room temperature using a STOE STADIP diffractometer (STOE, Darmstadt, Germany) equipped with a Mythen 2K linear detector. Data were collected in transmission mode (Debye–Scherrer geometry) in the 2θ ranges, 1.0–43.36° for 14 h using Mo Kα1 radiation (λ = 0.70930 Å). Samples were loaded in 0.5 and 0.7-mm special glass capillaries.

All Raman spectra were measured at 20 °C on a Renishaw In-Via Qontor Confocal Raman microscope (Renishaw, Wotton-under-Edge, United Kingdom). Point maps featured three sample areas, and five spectra were collected at each point. Point maps used a 532 nm laser with 1800 (mm) grating, 10 s of exposure time, 1% laser power, at 50× magnification, and five accumulations. Point maps were processed with cosmic ray and background removal and averaged. Wire software was used for data processing. For the *operando* Raman experiment, electrodes were prepared by casting onto 16 mm Al mesh. The electrode slurry was a composite of active material (60 wt %), super C65 carbon (30 wt %), and sodium carboxymethyl cellulose (CMC) binder (10 wt %). Using a pestle and mortar, the active material and conductive carbon were hand-ground together. The resulting powder was then added to the aqueous binder, which was prepared in a 1:45 (w/w) aqueous solution and mixed overnight. A few drops of the slurry were then deposited onto a mylar sheet, and the Al mesh was soaked until dry. The *operando* experiment was conducted using an Ivium compactstat B06023 potentiostat in cyclic voltammetry mode. The potential regions were from an open circuit voltage (OCV) of 1.47 V versus Na^+/Na to 0.01 V versus Na^+/Na to 2.5 V versus Na^+/Na at 0.2 mv s^{-1} and incremental step of 1 mV. One point was used throughout the experiment, and data collection occurred in 5 min increments.

EPR measurements were performed on a continuous wave Bruker EMX plus spectrometer (Bruker, USA) at X-band (9.5 GHz) at room temperature. Experiments were undertaken using 1 mW microwave power, 0.1 mT modulation amplitude, 100 kHz modulation frequency, 20 mT

Citation: *CCS Chem.* **2026**, Just Published. DOI: 10.31635/ccschem.026.202507155
Link to VoR: https://doi.org/10.31635/ccschem.026.202507155

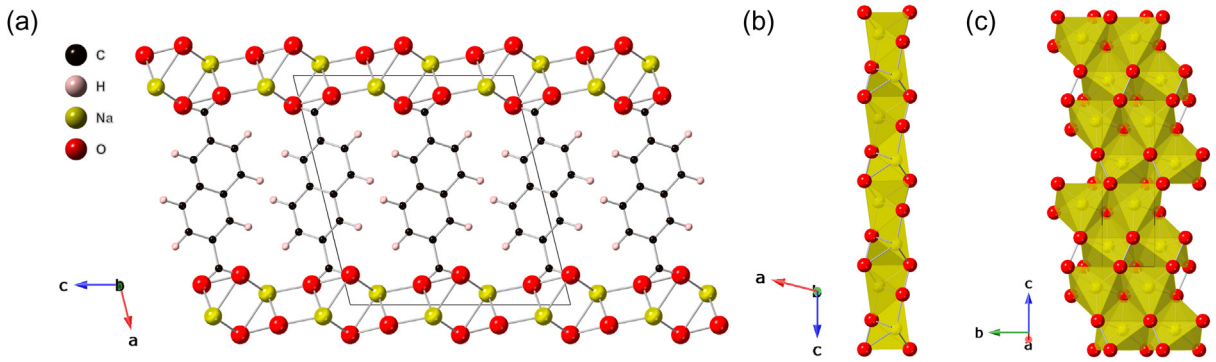

Figure 1 | *(a) View of Na_2NDC structure in the ac plane, expanded for clarity. The unit cell is shown in black. (b) Expanded view of Na^+–O distorted octahedra layer in the ac plane. (c) Expanded view of Na^+–O distorted octahedra in the bc plane. The unit cell is shown in black. In (b) and (c), the distorted NaO_6 octahedra are depicted as polyhedra, rather than the ball and stick representation shown in (a).*

field sweep centered at 350 mT with 600 points resolution, a time constant of 2.56 ms, and a conversion time of 13.34 ms. Samples were packed in 0.7-mm special glass capillaries, which were then loaded into a 4 mm Suprasil (Heraeus, Germany) EPR tube.

Experimental details on the 3D ED experiment, the PDF experiment including processing, analysis, and the calculation of the dPDF and the AIRSS procedure can be found in the Supporting Information.

Results and Discussion

3D ED structure of Na_2NDC

A previous attempt to solve the structure of Na_2NDC was an ab-initio structure solution from synchrotron powder diffraction data.[15] Whilst being a robust technique, single crystal structure solution remains preferable, due to being a direct structural solution from a three-dimensional dataset. The difficulty in growing single crystals of a suitable size, due to the material's highly ionic nature, meant that traditional single-crystal X-ray diffraction (SC-XRD) was not possible.[16] An alternative single-crystal technique, which does not require large crystallites, is 3D ED. 3D ED offers the ability for structure solution for crystals that are orders of magnitude smaller than those used for traditional SC-XRD.[16] Using the 3D ED technique, the structure of Na_2NDC was solved (details in Supporting Information Tables S1 and S2). The 3D ED structure was confirmed by performing a Rietveld refinement against PXRD data (Supporting Information Figure S1). Na_2NDC has a monoclinic unit cell in the $P2_1/c$ space group with unit cell parameters a = 12.136(3) Å, b = 3.5788 (8) Å, c = 11.3183(15) Å, β = 104.014(19)°. The structure can be described as featuring repeating layers of inorganic Na^+–O polyhedra, with distorted octahedral Na^+ environments. Na^+–O bond lengths vary from 2.34 to 2.67 Å. The inorganic layers are separated by naphthalene units, which are arranged in a π stacking arrangement in the b direction (Figure 1a–c). The π stacking distance is 3.58 Å, which is a standard distance for π stacking. In the c direction, the naphthalene units are orientated in alternating zig–zag fashion (Figure 2a,b). Evidently, 3D ED is an effective technique for solving the structure of microcrystalline materials and can be successfully applied to organic dicarboxylates, providing a route to single-crystal structure solution of challenging samples.

Ex situ PXRD of cycled Na_2NDC electrodes

Initial studies investigated the structural transformations of Na_2NDC upon electrochemical cycling using conventional ex situ PXRD. In this case, PXRD data were collected after discharging and charging half-cells to a particular voltage (see experimental for further details). Upon discharge in a sodium half-cell, the Na_2NDC system undergoes Na^+ insertion, promoting structural changes. The PXRD pattern collected at complete discharge of 0.01 V versus Na^+/Na illustrated that there was a large increase in disorder after Na^+ insertion, visible from the lack of Bragg peaks, a substantial broadening of existing Bragg peaks, and an increase in the amorphous background (Figure 3). This is in agreement with the work of Caroff et al.[17] The lack of long-range order means that conventional crystallographic analysis, such as Rietveld refinement, was not possible due to a lack of Bragg peaks. A second half-cell was discharged to 0.01 V versus Na^+/Na and then charged to 2.5 V versus Na^+/Na, so the Na_2NDC electrode underwent an initial Na^+ insertion followed by Na^+ extraction. The PXRD pattern collected after being charged to 2.5 V versus Na^+/Na showed that some of the reflections corresponding to Na_2NDC were present, alongside a persistent amorphous background in the PXRD pattern (Figure 3). Further analysis of the discharged sample is limited by a combination of the broadened Bragg peaks and the amorphous feature

Citation: *CCS Chem.* **2026**, Just Published. DOI: 10.31635/ccschem.026.202507155
Link to VoR: https://doi.org/10.31635/ccschem.026.202507155

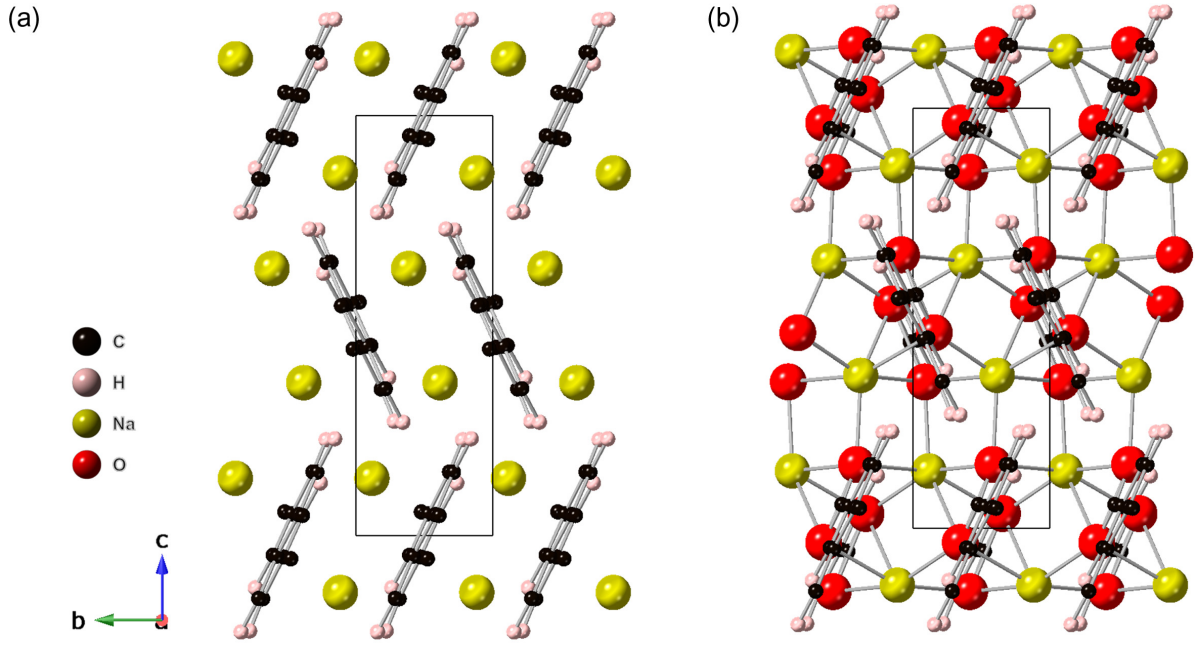

Figure 2 | *(a) Expanded view in the bc plane of the Na_2NDC structure, depicting the nature of the π stacking. O omitted for clarity. The unit cell is shown in black. (b) Expanded view in the bc plane of Na_2NDC structure depicting the nature of the π stacking with O included. The unit cell is shown in black.*

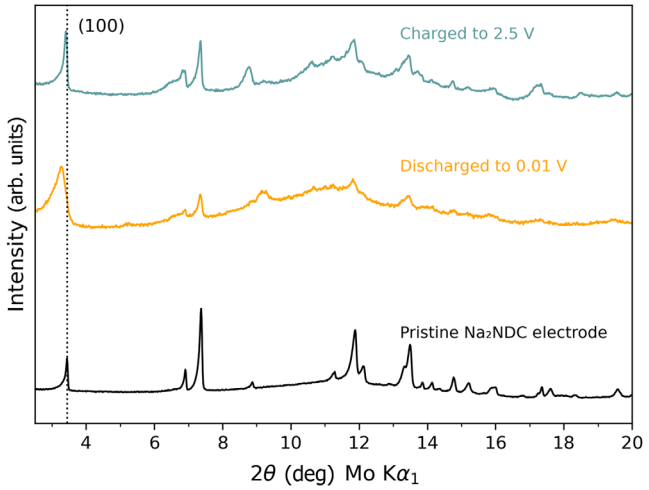

Figure 3 | *Ex situ PXRD patterns of the pristine Na_2NDC electrode, the Na_2NDC electrode after discharging to 0.01 V vs Na^+/Na, and discharging to 0.01 V vs Na^+/Na then charging to 2.5 V vs Na^+/Na.*

present, both indicating an increase in disorder in the system.

Operando Raman spectroscopy

Operando Raman spectroscopy was utilized to understand the evolution in the local structure of Na_2NDC upon electrochemical Na^+ insertion and extraction. The *operando* experiment consisted of one cyclic voltammetry sweep at 0.2 mV s^{-1}, in combination with the collection of Raman spectra in 5 min increments. The Raman spectrum of the electrode before cycling was similar to the Raman spectrum of pristine Na_2NDC; some signal contribution from the carbon additive was present as broad features at 1580 and 1680 cm^{-1}. Upon discharge, the voltammogram exhibited a peak at 0.5 V versus Na^+/Na, which, on continued discharge to lower potential, led to the formation of another peak at 0.03 V versus Na^+/Na. The first changes to the Raman spectra occurred at 0.33 V versus Na^+/Na, where there was a rapid change in the Raman spectrum. Peaks attributed to the Na_2NDC phase reduced in intensity until they disappeared, concurrently new peaks appeared and then increased in intensity. The transformation of the Raman spectra was complete after discharging to 0.09 V versus Na^+/Na, with no evidence of pristine Na_2NDC and a different Raman signature present (Figure 4a–c). The new Raman spectrum is attributed to s-NDC and is attributed to the large peak observed in the voltammogram. Continued discharge to 0.01 V versus Na^+/Na illustrated no further changes to the Raman spectra, with no apparent contribution from the carbon additive. Upon charge, the voltammogram illustrated a small peak at 0.40 V versus Na^+/Na, and a large peak at 0.60 V versus Na^+/Na. The Raman spectrum was unchanged until 0.69 V versus Na^+/Na. At 0.69 V versus Na^+/Na, the intensity of peaks attributed to s-NDC decreased rapidly, and the Na_2NDC Raman spectrum rapidly reappeared. Overall, the

Citation: *CCS Chem.* **2026**, Just Published. DOI: 10.31635/ccschem.026.202507155
Link to VoR: https://doi.org/10.31635/ccschem.026.202507155

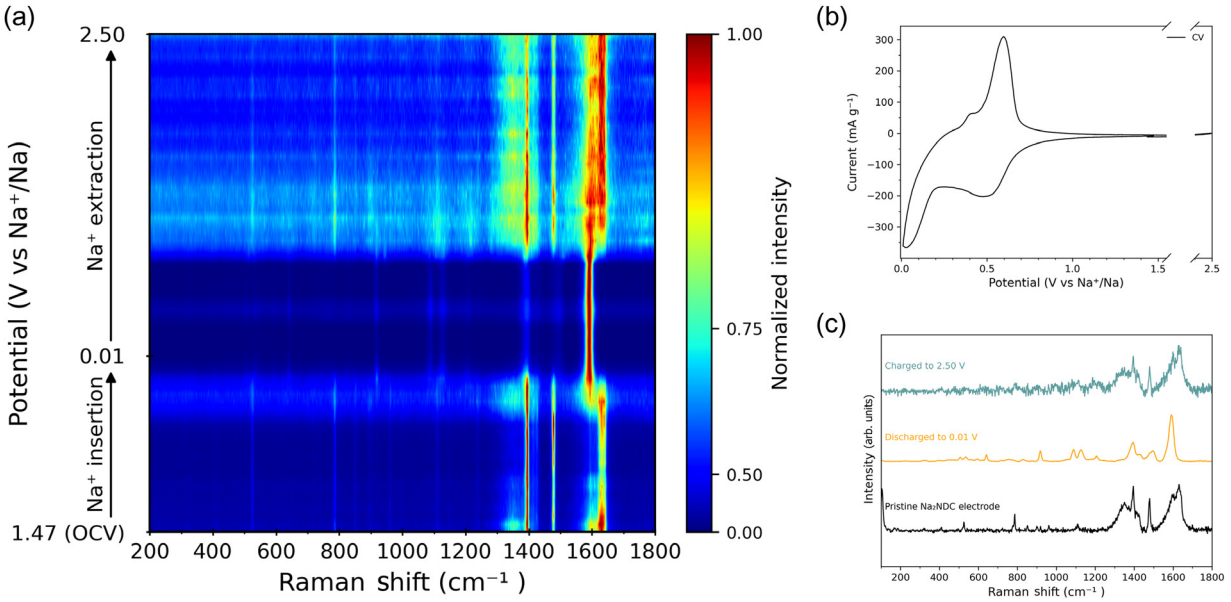

Figure 4 | *(a) Contour map of operando Raman data during discharging and charging of the Na_2NDC electrode from OCV of 1.47 V vs Na^+/Na to 0.01 V vs Na^+/Na to 2.5 V vs Na^+/Na in a cyclic voltammetry experiment at a scan rate of 0.2 mV/s. (b) Cyclic voltammogram from the operando Raman experiment. (c) Comparison of the Raman spectrum of the pristine Na_2NDC electrode and at 0.01 V vs Na^+/Na and 2.5 V vs Na^+/Na from the operando Raman experiment.*

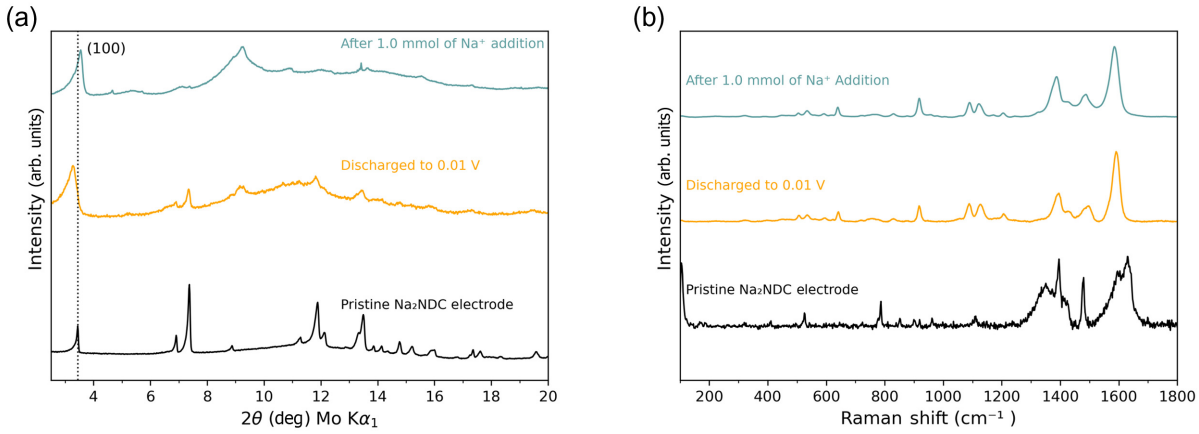

Figure 5 | *(a) Ex situ PXRD pattern of Na_2NDC, compared with an ex situ Na_2NDC electrode sample after discharge to 0.01 V vs Na^+/Na and the chemical sodiation product. (b) Operando Raman spectrum of pristine Na_2NDC electrode compared with the operando Na_2NDC electrode sample after discharging to 0.01 V, and the chemical sodiation product. The chemical sodiation conditions were 1.0 mmol of reducing agent added to 0.16 mmol of Na_2NDC. Voltages are vs Na^+/Na.*

operando Raman data illustrate a reversible reaction mechanism. The *operando* Raman data also revealed that there is a locally consistent s-NDC structure during Na^+ insertion, shown by the presence of one s-NDC spectrum throughout the entirety of the *operando* experiment. The Na^+ insertion and extraction mechanism appears to be biphasic, demonstrated by the presence of two distinct Raman spectra throughout the *operando* experiment. This is in agreement with previous work on Na_2NDC, which suggested a 2-electron, 2-Na^+ insertion process (Supporting Information Figure S2). The biphasic mechanism suggested by the *operando* Raman experiment is in agreement with the plateau in the capacity-voltage profile of Na_2NDC, confirming a biphasic mechanism (Supporting Information Figure S3).

Citation: *CCS Chem.* **2026**, Just Published. DOI: 10.31635/ccschem.026.202507155
Link to VoR: https://doi.org/10.31635/ccschem.026.202507155

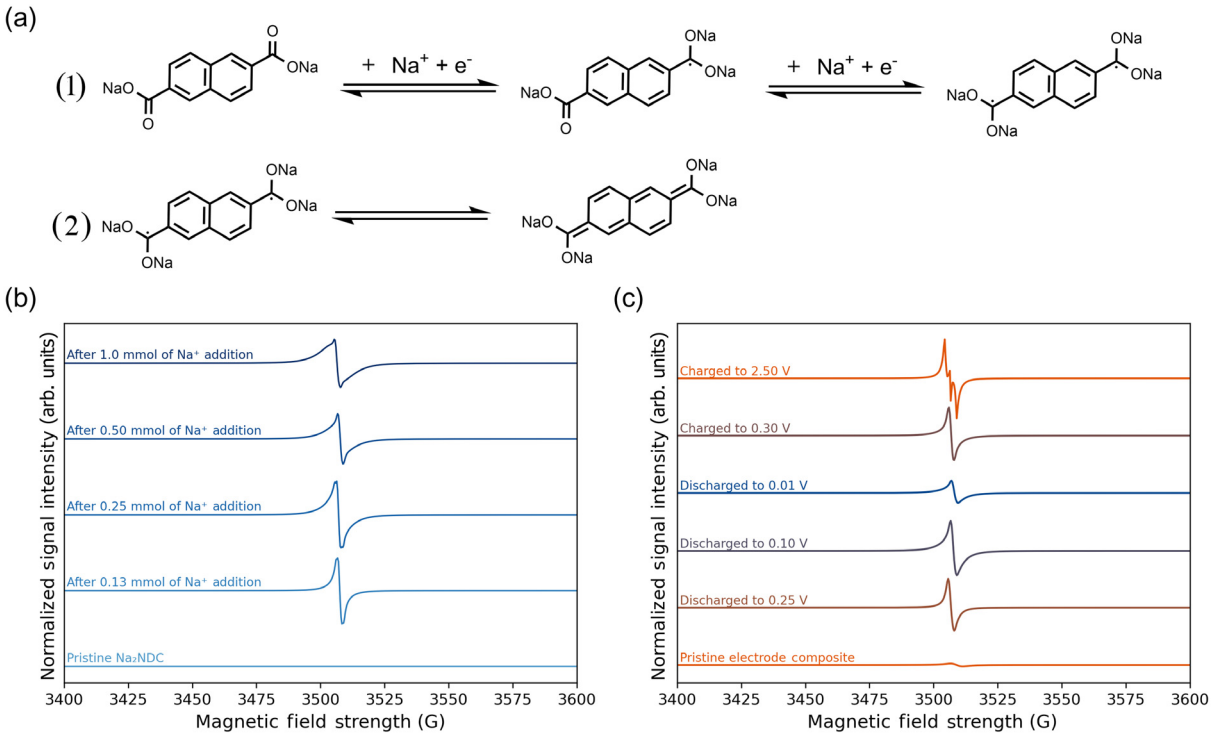

Figure 6 | *(a) (1) Reaction scheme depicting the radical redox mechanism of Na_2NDC when undergoing Na^+ insertion (2) Resonance structures depicting radical reorganization to achieve aromaticity for s-NDC (b) Ex situ EPR spectra of discharged and charged Na_2NDC electrode samples after cycling in sodium half cells. (c) Ex situ EPR spectra of pristine Na_2NDC and the chemical sodiation product after 0.13, 0.25, 0.5, and 1 mmol of reducing agent addition to 0.17–0.19 mmol of Na_2NDC. Voltages are vs Na^+/Na.*

Chemical sodiation of Na_2NDC

One of the difficulties in studying organic electrode materials stems from the fact that electrodes are composites of active materials, binders, and conductive additives. As the elemental composition of the binders and conductive additives is comparable to the active organic electrode material, it can be difficult to separate these contributions when carrying out structural characterization. Here, a chemical sodiation procedure was used to chemically insert Na^+ into Na_2NDC to produce s-NDC to allow the study of the material without any signal contribution from binders or conductive additives. The chemical sodiation procedure aimed to emulate the electrochemical Na^+ insertion reaction of Na_2NDC. The reducing agent of choice was the widely used NaBP. The negative reduction potential of NaBP illustrates its efficacy as a reducing agent.[21] The theoretical Na^+ insertion required to produce Na_4NDC is a 2-electron, 2-Na^+ insertion process (Supporting Information Figure S2).[15] The molar ratio between the amount of NaBP reducing agent used and the moles of Na^+ inserted is 1:1. Therefore, a 2:1 molar ratio of reducing agent to Na_2NDC is required for the complete conversion of Na_2NDC to Na_4NDC. To ensure full reaction conversion, an excess of reducing agent was used. To verify the success of the chemical sodiation procedure, PXRD patterns and Raman spectra of the chemical sodiation product were collected to compare against the electrochemically sodiated data (Figure 5). The PXRD pattern of the chemically sodiated product and the ex situ Na_2NDC electrode that had been discharged to 0.01 V versus Na^+/Na were similar. Both PXRD patterns showed a significant increase in disorder and the persistence of the (100) reflection (Figure 5a). The Raman signature of the chemically sodiated product and the *operando* Na_2NDC sample that was discharged to 0.01 V versus Na^+/Na was also similar (Figure 5b). The similarities between the PXRD patterns and Raman spectra of the chemically and electrochemically sodiated products confirmed the successful chemical sodiation of Na_2NDC to the identical s-NDC product regardless of the method of sodiation.

Ex situ EPR results

To understand if there was any radical formation during Na^+ insertion, ex situ EPR spectra of the chemically and electrochemically sodiated samples were measured. The closed shell Na_4NDC species postulated by Cabañero Jr et al.[15] would not possess any EPR signal. However, a

Citation: *CCS Chem.* **2026**, Just Published. DOI: 10.31635/ccschem.026.202507155
Link to VoR: https://doi.org/10.31635/ccschem.026.202507155

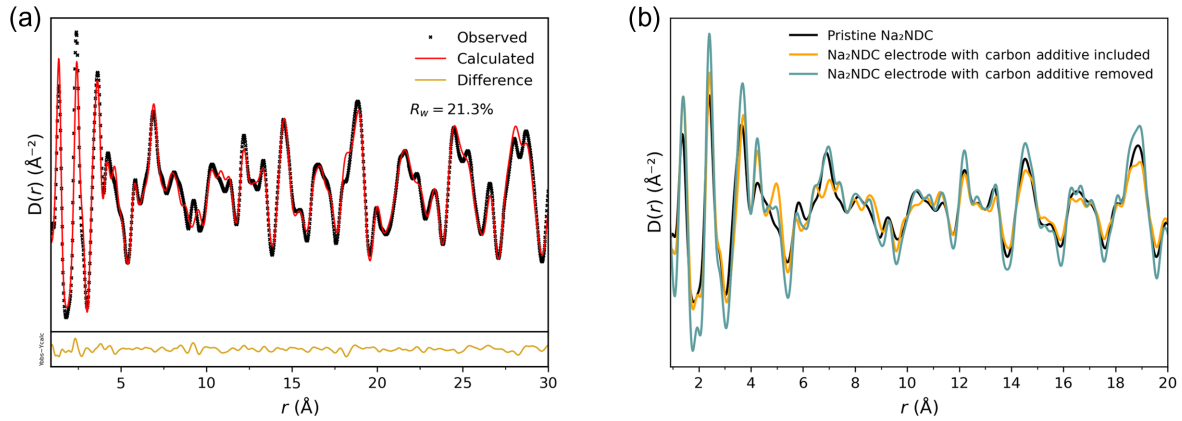

Figure 7 | *(a) Real-space least squares refinement of the Na_2NDC structure (obtained from 3D ED data) refined against experimental PDF data of Na_2NDC. Black crosses depict the observed data points. Red line depicts calculated fit. Gold line depicts difference between the observed and calculated data. (b) Experimental PDF data of pristine Na_2NDC, the electrode with the carbon additive included in the PDF, and with the carbon additive removed from the PDF during processing.*

partially sodiated Na_{2+x}NDC ($0<x<2$) structure would possess an EPR signal. The radical structure would likely feature the radical centered on the carboxylate carbon due to the reduction of the carbonyl upon Na^+ insertion (Figure 6a). Using 0.17–0.19 mmol of Na_2NDC, four experimental chemical sodiation batches were created, with each experimental batch featuring a different amount of Na^+ addition. The experimental set featured samples having 0.13, 0.25, 0.5, and 1 mmol of reducing agent added, respectively. Pristine Na_2NDC does not possess any EPR signal (Figure 6b). The chemically sodiated products all displayed an EPR signal, demonstrating that a stable radical environment is present in s-NDC (Figure 6b). The ex situ EPR spectra of the chemically sodiated samples suggest that a radical Na_{2+x}NDC state exists upon Na^+ insertion into Na_2NDC and not the closed shell Na_4NDC previously suggested by Cabañero Jr et al.,[15] unless Na_4NDC is a stable dual radical species (Figure 6a). The stability of the naphthalene-based radical may be due to the reasons postulated by Wu et al.[22] Their claim was that a rigid organic structure with extended conjugation contributed to the stability of organic radicals.[22] The pristine Na_2NDC electrode exhibited a small signal stemming from the conductive carbon additive, which has been previously reported.[23] Upon discharge, there is an increase in the intensity of the EPR signal, illustrating an increase in the number of unpaired electron spins. This reaches its maximum intensity at 0.1 V versus Na^+/Na (Figure 6c). The Na^+ insertion of Na_2NDC is likely responsible for the increase in the number of spins, considering that the voltage profile shows the Na^+ insertion process into Na_2NDC to be electrochemically active before 0.1 V versus Na^+/Na (Supporting Information Figure S3). Continued discharge to lower potentials results in a decrease in the intensity of the EPR signal, corresponding to a decrease in the number of unpaired spins. At 0.01 V, the EPR signal decreases, suggesting complete or near complete sodiation of Na_2NDC to a closed shell Na_4NDC, possibly with some Na_{2+x}NDC remaining. The lineshape of the EPR signal resembles previously reported carbon-based radicals, such as those from Wang et al.[22] and Wu et al.,[24] in ex situ studies of carbonaceous and organic electrodes, respectively. Upon charge, there is an increase in the EPR signal, and at complete charge, (2.5 V vs Na^+/Na), this splits into a second peak which has been previously reported.[25] The broad signal at 2.5 V versus Na^+/Na is likely derived from the organic radical, illustrating that on charge, there is a residual radical signal in the sample. Therefore, the conversion from the s-NDC structure to Na_2NDC upon Na^+ extraction appears to be incomplete, terminating at a Na_{2+x}NDC stoichiometry. The ex situ EPR results suggest that both electrochemical and chemical Na^+ insertion into Na_2NDC produces a radical Na_{2+x}NDC state, with the chemical sodiation product unable to reach complete sodiation to produce Na_4NDC, while some Na_4NDC appears to be produced from the electrochemical Na^+ insertion. This is likely due to the rapid reaction kinetics of the chemical sodiation reaction. The chemical sodiation reaction takes 1 min, compared to the electrochemical sodiation which takes nearly 33 h at 10 mA g^{-1}.

Ex situ PDF results

Ex situ PDF experiments were conducted to gain insight into the structural changes that occur to Na_2NDC upon Na^+ insertion and to postulate a sodiation mechanism. The PDF is a weighted histogram of all the atom–atom

Citation: *CCS Chem.* **2026**, Just Published. DOI: 10.31635/ccschem.026.202507155
Link to VoR: https://doi.org/10.31635/ccschem.026.202507155

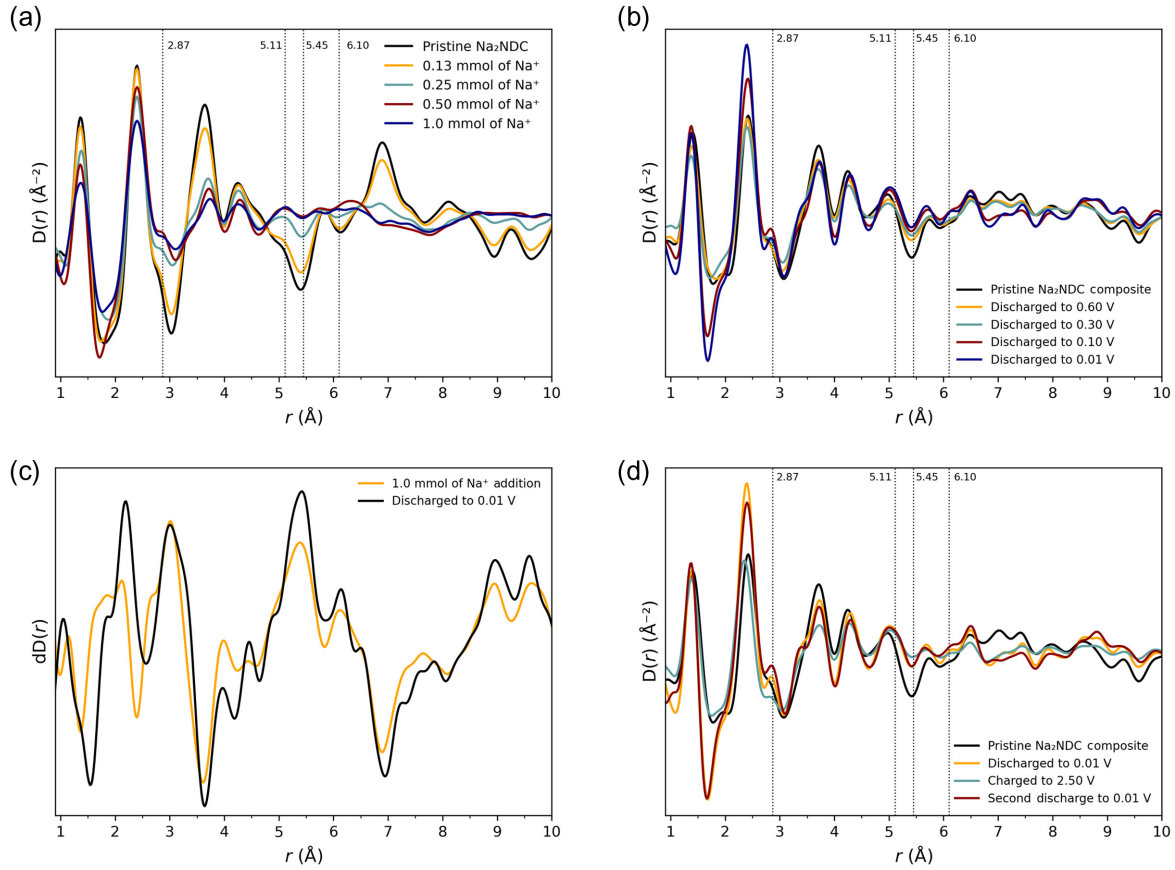

Figure 8 | *(a) Experimental PDF data of pristine Na_2NDC and the chemical sodiation product after 0.13, 0.25, 0.5, and 1 mmol of reducing agent addition to 0.15–0.17 mmol of Na_2NDC. (b) Experimental PDF data for Na_2NDC electrodes after discharging in sodium half cells. (c) dPDF data of the chemical and electrochemical sodiation products. (d) Experimental PDF data for Na_2NDC electrodes after discharging, charging, and second discharge in sodium half cells. Voltages are vs Na^+/Na.*

distances in a material and is a short and medium range structural probe suitable for studying disordered materials. PDF is ideal for studying s-NDC because it is disordered, as revealed by PXRD (Figure 3). The ex situ experiments consisted of collecting data of pristine samples and standards, which was then followed by measuring the PDFs of samples sodiated by both electrochemical and chemical means. First, a real-space least-squares refinement of the 3D ED Na_2NDC structure was conducted against the experimental PDF of Na_2NDC to verify the accuracy of using PDF on the Na_2NDC system (Figure 7a). The refinement showed good agreement between experimental and calculated patterns (Further details in the Supporting Information). The refined structure closely resembles the starting model confirming the accuracy of the Na_2NDC structure and the utility of PDF to study molecular organics such as Na_2NDC, in agreement with the work of Prill et al.[26] To be aware of the contribution of the carbon additive, the PDF of the pristine Na_2NDC electrode was generated with and without the contribution of the carbon additive, and compared to the PDF of pristine Na_2NDC (Figure 7b). The PDF with the carbon additive included is dominated by Na_2NDC due to the larger amount present in the electrode (70:30 ratio of Na_2NDC: carbon additive by weight).

Using 0.15–0.17 mmol of Na_2NDC, four experimental chemical sodiation batches were created, with each experimental batch featuring a different amount of Na^+ addition. The experimental set featured samples having 0.13, 0.25, 0.5, and 1 mmol of reducing agent added, respectively. Total scattering data were then collected of the four chemical sodiation products and the corresponding PDFs generated to observe the local structural changes that occur as a function of Na^+ insertion. Upon the addition of the smallest amount of reducing agent (0.13 mmol), the PDF does not visibly change (Figure 8a). Addition of a greater amount of reducing agent (0.25 mmol) to Na_2NDC led to new peaks appearing at 2.87, 5.11, 5.45, and 6.10 Å. There is a reduction in the intensity of peaks at 3.63, 4.25, and 6.89 Å (Figure 8a). The transformation appears complete after the addition

Citation: *CCS Chem.* **2026**, Just Published. DOI: 10.31635/ccschem.026.202507155
Link to VoR: https://doi.org/10.31635/ccschem.026.202507155

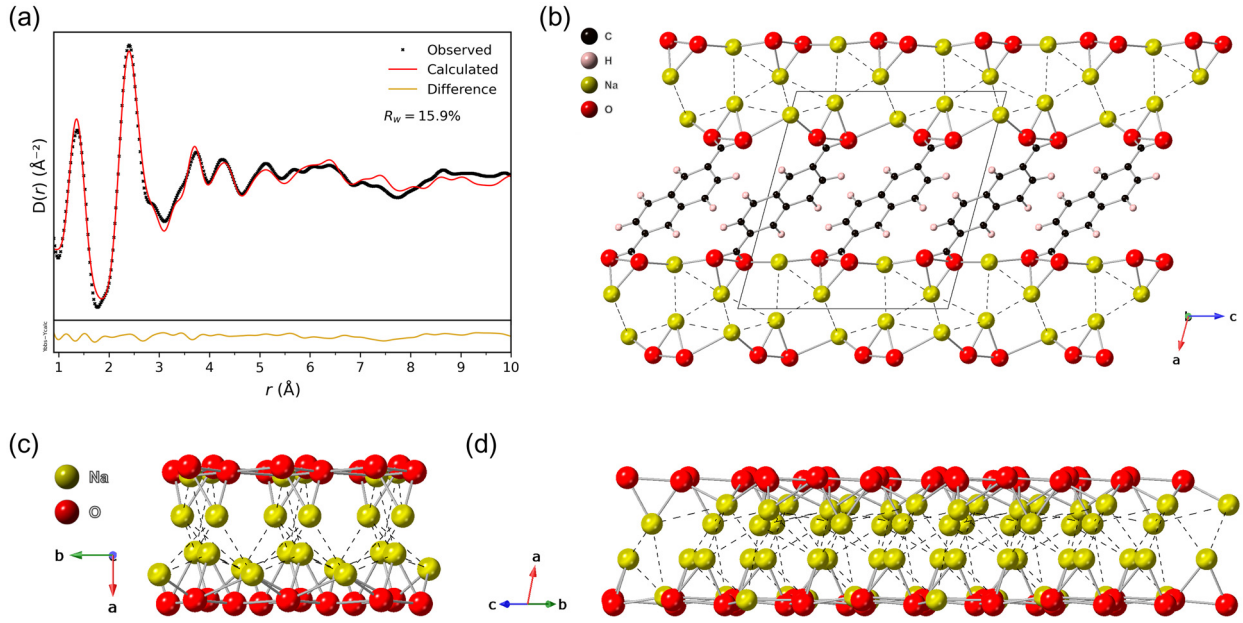

Figure 9 | *(a) Real-space least squares refinement of a P1 Na_{2+x}NDC model against experimental PDF data for a chemically reduced sample after 1 mmol of reducing agent was added to 0.16 mmol of Na_2NDC. Black crosses depict the observed data points. Red line depicts the calculated fit. Gold line depicts the difference between the observed and calculated data. (b) Expanded view of the P1 s-NDC structure in the ac plane. The unit cell is shown in black. (c) View of the s-NDC inorganic layer in the ab plane. (d) Expanded view of the s-NDC inorganic layer.*

of 0.5 mmol of reducing agent, which would correspond to the insertion of approximately 2 Na^+ per Na_2NDC unit, and therefore the theoretical Na_4NDC product. There is the loss of long-range order, evidenced by the lack of peaks beyond 10 Å (Supporting Information Figure S4), and this is in agreement with the PXRD pattern visible in Figure 3. There is an increase in the intensity of peaks at 2.87, 5.11, 5.45, and 6.10 Å, analogous to the 0.25 mmol sample. There is also the same decrease in intensity of peaks as for the 0.25 mmol sample, observed at 3.63, 4.25, and 6.89 Å (Figure 8a). Once an excess of reducing agent (1 mmol) is added, the PDF does not change significantly. The similarities between the PDFs confirm the success of the sodiation procedure after 0.5 mmol of Na^+ was added. dPDF shows a continual trend in the evolution of the PDFs (Supporting Information Figure S5) as the consumption of Na_2NDC occurs to produce the s-NDC phase, with the change of peaks at low *r* and the loss of peaks at high *r*. The trend follows the increased amount of reducing agent that was added and the consequent proportion of s-NDC increasing. The dPDF reveals that some s-NDC is present when a minority of reducing agent is added (0.13 mmol), although the PDF itself visibly appears to be unchanged, thus illustrating the accuracy and sensitivity of the technique. The next phase of the study was to collect data on ex situ samples of Na_2NDC after electrochemical Na^+ insertion and extraction (by discharging and charging in sodium half-cells). We also collected PDF data after the second Na^+ insertion (second discharge in a sodium half-cell). For the first cycle, after discharge to 0.6 V versus Na^+/Na, the PDF showed no visible change (Figure 8b and Supporting Information Figure S6). This is likely because the only major process to occur at this voltage is the formation of the solid electrolyte interphase (SEI), driven by the conductive additive, making up a minority of the overall electrode (Supporting Information Figure S3). When discharged to 0.3 V versus Na^+/Na, there were small changes to the PDF. Further discharge to 0.1 V versus Na^+/Na resulted in a significant change to the PDF as the primary Na^+ insertion process into Na_2NDC occurs (Figure 8b and Supporting Information Figure S6). New peaks appeared at 2.87, 5.45, and 6.10 Å. Peaks reduced in intensity at 3.63, 4.25, and 6.89 Å. The transformation in peaks is identical to that observed for chemical sodiation and is likely due to the consumption of Na_2NDC and the formation of s-NDC. After discharge to 0.01 V versus Na^+/Na, the primary features of the s-NDC PDF remain (Figure 8b and Supporting Information Figure S6). Figure 8c shows differential experimental dPDF data of the chemical sodiation product and the electrochemical sodiation product. The comparison of the PDFs can be seen in Supporting Information Figure S7. The dPDF for the chemically sodiated sample was calculated by subtracting the PDF of pristine Na_2NDC from the PDF after 1 mmol of Na^+ addition. The dPDF of the electrochemically sodiated sample was calculated by

Citation: *CCS Chem.* **2026**, Just Published. DOI: 10.31635/ccschem.026.202507155
Link to VoR: https://doi.org/10.31635/ccschem.026.202507155

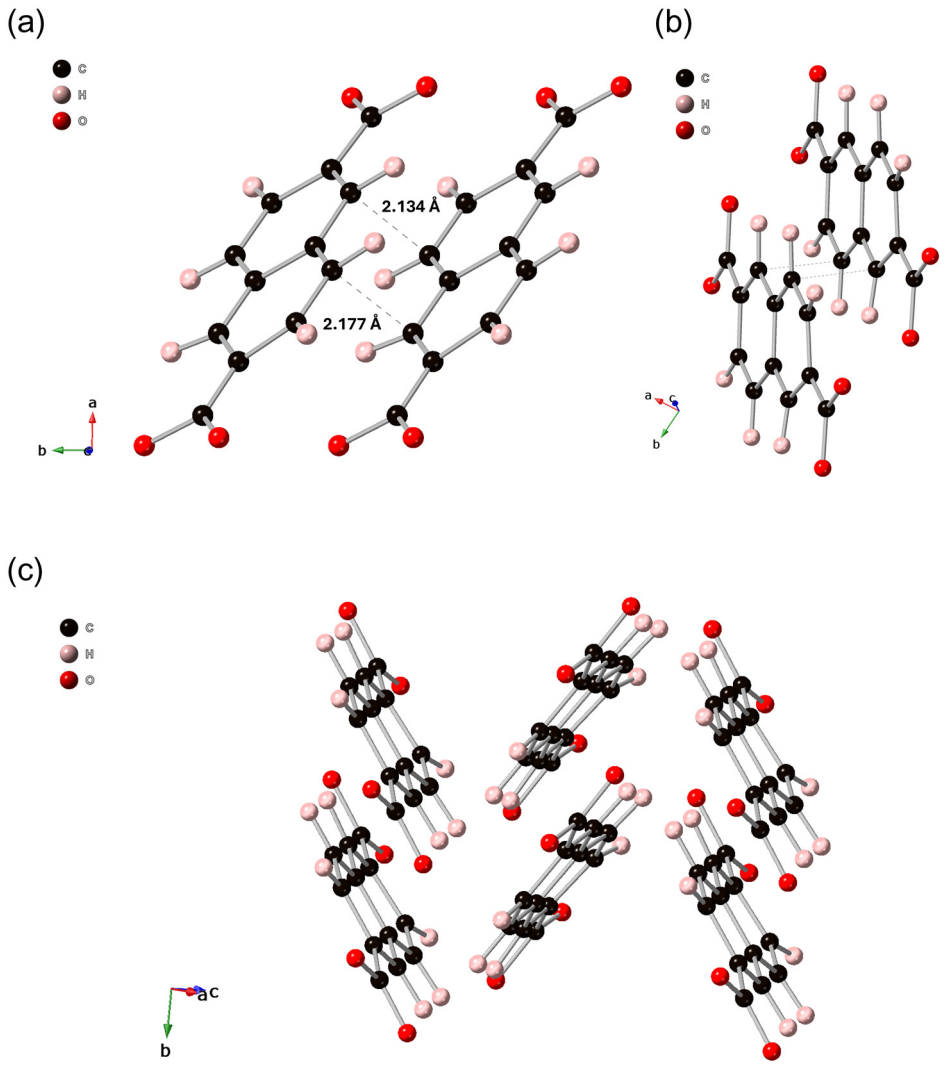

Figure 10 | *(a) The naphthalene units in s-NDC after reorientation. Offset view. Na omitted for clarity. (b) The naphthalene units in s-NDC after reorientation. Offset ab view. Na omitted for clarity. (c) The naphthalene units in s-NDC after reorientation. Offset view. Na omitted for clarity.*

subtracting the PDF of the pristine Na_2NDC electrode from the PDF of the electrode after discharge to 0.01 V (see Supporting Information). The PDFs of the pristine and discharged electrodes in this instance were generated by also subtracting the pristine carbon additive to remove its contribution from the dPDF. A comparison of the dPDFs illustrate highly comparable changes as a result of Na^+ in accordance with the PXRD and Raman data (Figures 3 and 4). Therefore, samples that were chemically and electrochemically sodiated undergo comparable changes in local structure upon sodiation. Notably, after both chemical and electrochemical Na^+ insertion, the peak at 1.36 Å is relatively unaltered throughout, which corresponds to the C–C and C–O bonds of the naphthalene unit, signifying the retention of the intramolecular naphthalene bonding framework. Upon charge, the only significant change occurred at 2.87 Å, suggesting that this distance is associated with a Na^+-atom distance (Figure 8d). The PDFs of the discharged and charged samples closely resemble one another (Figure 8d). There was no return of peaks at high *r*, indicating no return of long-range order. Upon a second discharge, the only significant change in the PDF is an increase in the intensity of the peak at 2.87 Å. The similarities in the PDF after discharge, charge, and second discharge suggest a major structural change only upon the first sodiation. The repeated increase and decrease of a single peak at 2.87 Å after the first Na^+ insertion provides validation that there are minor structural changes upon repeated cycling of Na_2NDC.

Structural insights from PDF modeling

To obtain insight into the structure of s-NDC, potential model structures were generated using AIRSS.[19,20] The 20 lowest energy AIRSS structures then underwent a

Citation: *CCS Chem.* **2026**, Just Published. DOI: 10.31635/ccschem.026.202507155
Link to VoR: https://doi.org/10.31635/ccschem.026.202507155

geometry optimization using DFT and could be grouped into three structure types. Two structure types were $P2_1$ unit cells and one was a *Pc* unit cell. The selected models were then used as a starting point for the simulated annealing and real-space least-squares refinement procedure. The simulated annealing and real-space least-squares refinement procedure was conducted against the experimental PDF data of the chemical sodiation product after 1 mmol of reducing agent was added to 0.16 mmol of Na_2NDC. The structure type that gave the best fit after annealing and the most appropriate chemical result was the structure with the unit cell in the *Pc* space group, which subsequently underwent a real-space least-squares refinement. The resulting *Pc* unit cell and structure was then relaxed to the *P*1 space group to remove symmetry constraints and underwent a repeat of the simulated annealing and refinement procedure (Supporting Information Figure S8). The purpose of repeating the simulated annealing procedure was to accommodate disorder in the inorganic Na^+-O layer. The organic layer was fixed after refinement in the *Pc* cell to maintain an ordered π stacking arrangement. To completely explore the disorder in the inorganic Na^+-O layer, a 1×3×1 supercell was constructed. The size of the supercell was constructed so that all cell vectors were at least 10 Å long to enable a full description of the correlation length of the s-NDC, which is approximately 10 Å. The structure was subsequently annealed and refined again. All refinements showed excellent fits with the *Pc* unit cell having an R_w of 16.3%, *P*1 unit cell an R_w of 15.9%, and the supercell an R_w of 13.2% (Supporting Information Figure S8). Discussed herein is the *P*1 model (see Supporting Information Figure S9 for all models). The model revealed that the inorganic Na^+–O layer is responsible for Na^+ storage. The layer was retained but expanded in size (Figure 9a–d, Supporting Information Figures S10 and S11) to accommodate the inserted Na^+. The Na^+ occupied two different coordination environments, one is a distorted trigonal planar geometry and the other is two-coordinate, featuring the Na^+ positioned more centrally in the inorganic layer. The Na^+–O bond lengths vary between 2.16 and 2.97 Å. The two-coordinate Na^+ feature varied occupancies and is likely a highly mobile, disordered layer contributing to Na_2NDC's impressive rate performance in sodium half-cells. The refinement of the Na^+ occupancies of the *P*1 cell gave an s-NDC stoichiometry of $Na_{3.80}$NDC. The Na^+ insertion of 3.80 supports the suggestion that chemical sodiation is incomplete, hence the formation of a radical s-NDC species.

The modeling results show that the naphthalene units move closer together but shift relative to one another to form a parallel offset packing geometry. Carbon–carbon distances between naphthalene units approach as close as 2.13 and 2.18 Å (Figure 10a–c). The actual approach distance is not chemically feasible and is likely due to a combination of unit cell inaccuracy, not accounting for possible distortion of the naphthalene unit, and only modeling the individual naphthalene unit present in the *Pc* unit cell. The naphthalene unit was then fixed for subsequent simulated annealing and refinement in the *P*1 unit cell and supercell. However, the general approach and reorientation of the naphthalene units towards one another does appear to be a genuine structural motif of the s-NDC structure. We speculate that the cause of the close intermolecular distance of the naphthalene units is due to an interaction known as pancake bonding.[27–29] Pancake bonding arises in organic radical systems; the EPR spectra in Figure 6 have revealed the s-NDC system to be a stable radical environment. Pancake bonding occurs due to orbital overlap between the singly occupied molecular orbitals (SOMO) that are present in stacked radicals of π systems, such as in s-NDC. The SOMO–SOMO overlap results in a stabilization effect.[27–29] The stabilization effect results in the separate conjugated π species approaching at a closer distance than the Van der Waals (VdW) distance.[27–29] The combination of the EPR data with PDF modelling suggests that a close π–π stacking distance is present. Our results suggest a pancake bonding phenomenon is present in s-NDC.

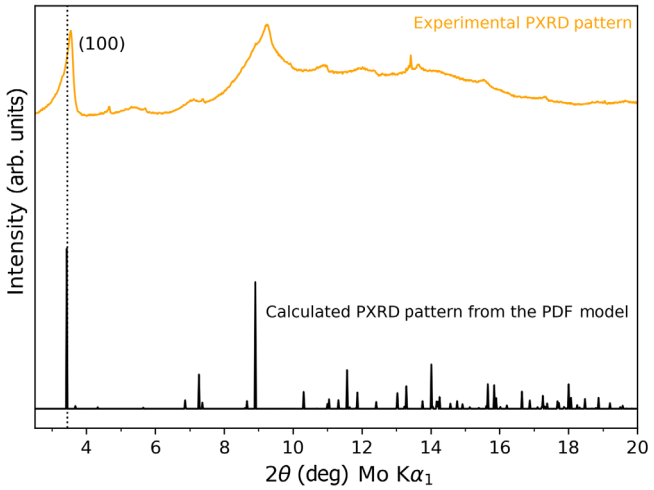

Figure 11 | *Experimental PXRD pattern for a chemically sodiated NDC sample (s-NDC), and the calculated PXRD pattern from the P1 PDF derived model.*

Evidence of the reliability of the PDF-derived model stems from the close match between the calculated and experimental PXRD patterns of s-NDC. The most intense reflections are in close agreement, as shown in Figure 11.

This multi-technique approach has shown that there is a similar Na^+ insertion mechanism for Na_2NDC regardless of the means of the sodiation. The Na_{2+x}NDC s-NDC species appears to have a variable composition depending on the extent of the sodiation, and it appears that a greater amount of sodiation can occur when Na_2NDC is sodiated electrochemically. The initial Na^+ insertion mechanism is biphasic and features the loss of long-

Citation: *CCS Chem.* **2026**, Just Published. DOI: 10.31635/ccschem.026.202507155
Link to VoR: https://doi.org/10.31635/ccschem.026.202507155

range order accompanied by significant rearrangement of the local structure. The inorganic Na^+–O layer is responsible for Na^+ storage, expanding to accommodate the inserted Na^+. The organic layer is retained, as is the naphthalene bonding framework, but each unit Reorientates in space to occupy a parallel offset geometry with respect to one another. The reorientation is likely the result of a π interaction known as pancake bonding driven by the existence of the naphthalene units as radical species and to assist in accommodating the inserted Na^+. After the structural rearrangement due to the first Na^+ insertion, minimal structural changes occur for repeated Na^+ insertion and extraction.

Conclusion

A path to elucidate the structural transformations that occur to an organic electrode material upon Na^+ insertion has been demonstrated. The approach featured the structure solution of Na_2NDC using 3D ED. Ex situ PXRD illustrated the structural disorder imparted by Na^+ insertion. *Operando* Raman spectroscopy revealed a consistent local structure throughout sodiation. The use of both techniques revealed the parity in the chemical and electrochemical sodiation products. Ex situ EPR showed that the chemical sodiation product is a stable organic radical and evidenced radical formation during discharge and charge of Na_2NDC electrodes. Ex situ PDF data and corresponding dPDF analysis of chemically and electrochemically sodiated samples revealed the fundamental structural changes that occurred upon Na^+ insertion are consistent regardless of the means of sodiation. Ex situ PDF data were in agreement with the ex situ PXRD data, which showed a loss of long-range order due to Na^+ insertion and appeared to show significant structural changes upon the first Na^+ insertion with subsequent Na^+ extraction and reinsertion resulting in minor changes to the PDF. A structure of the sodiated material has been postulated using a combined computational and experimental approach, incorporating the use of the AIRSS methodology as a starting point with a modeling approach using experimental PDF data. The postulated structural model revealed that Na^+ insertion occurs in the Na^+–O inorganic layer, causing its expansion, which coincided with a reorientation of the naphthalene layer. It appears that the reorientation of the naphthalene layer is also promoted by the presence of a naphthalene radical, which leads to a close π interaction phenomenon known as pancake bonding. We have demonstrated that PDF can be used to study organic electrode materials and can be used to investigate the structure after Na^+ insertion. Overall, this study is an important step in developing strategies to shed light on the Na^+ insertion mechanism of organic electrode materials.

Supporting Information

Supporting Information is available and includes further experimental information and data.

Conflict of Interest

There is no conflict of interest to report.

Acknowledgments

The authors acknowledge the assistance of Diamond Light Source for access to I15-1 beamline under proposal CY36333. The authors acknowledge the support from Engineering and Physical Sciences Research Council (EPSRC) Core Equipment Grant (EP/V034138/1) for powder diffractometers. We gratefully acknowledge funding from the EPSRC through grant number EP/T019298/1. The authors thank the Faraday Institution for funding (grants—FIRG018, FIRG064). H.S.S thanks the Allan Handsel Postgraduate Research Scholarship for Chemistry for funding. D.N.R thank the EPSRC (EP/X014444/1, and EP/X014606/1), for funding.

References

1. Li, X.; Wang, Y.; Lv, L.; Zhu, G.; Qu, Q.; Zheng, H. Electroactive Organics as Promising Anode Materials for Rechargeable Lithium Ion and Sodium Ion Batteries. *Energy Mater.* **2022**, *2*, 200014.
2. Liedel, C. Sustainable Battery Materials from Biomass. *ChemSusChem* **2020**, *13*, 2110–2141.
3. Poizot, P.; Gaubicher, J.; Renault, S.; Dubois, L.; Liang, Y.; Yao, Y. Opportunities and Challenges for Organic Electrodes in Electrochemical Energy Storage. *Chem. Rev.* **2020**, *120*, 6490–6557.
4. Desai, A. V.; Rainer, D. N.; Pramanik, A.; Cabañero, J. M. Jr.; Morris, R. E.; Armstrong, A. R. Rapid Microwave-Assisted Synthesis and Electrode Optimization of Organic Anode Materials in Sodium-Ion Batteries. *Small Methods* **2021**, *5*, 2101016.
5. Rajagopalan, R.; Tang, Y.; Jia, C.; Ji, X.; Wang, H. Understanding the Sodium Storage Mechanisms of Organic Electrodes in Sodium Ion Batteries: Issues and Solutions. *Energy Environ. Sci.* **2020**, *13*, 1568–1592.
6. Desai, A. V.; Morris, R. E.; Armstrong, A. R. Advances in Organic Anode Materials for Na-/K-Ion Rechargeable Batteries. *ChemSusChem* **2020**, *13*, 4866–4884.
7. Wu, X.; Jin, S.; Zhang, Z.; Jiang, L.; Mu, L.; Hu, Y.-S.; Li, H.; Chen, X.; Armand, M.; Chen, L.; Huang, X. Unraveling the Storage Mechanism in Organic Carbonyl Electrodes for Sodium-Ion Batteries. *Sci. Adv.* **2015**, *1*, e1500330.
8. Allan, P. K.; Griffin, J. M.; Darwiche, A.; Borkiewicz, O. J.; Wiaderek, K. M.; Chapman, K. W.; Morris, A. J.; Chupas, P. J.; Monconduit, L.; Grey, C. P. Tracking Sodium-Antimonide Phase Transformations in Sodium-Ion Anodes: Insights from

Citation: *CCS Chem.* **2026**, Just Published. DOI: 10.31635/ccschem.026.202507155
Link to VoR: https://doi.org/10.31635/ccschem.026.202507155

Operando Pair Distribution Function Analysis and Solid-State NMR Spectroscopy. *J. Am. Chem. Soc.* **2016**, *138*, 2352–2365.
9. Stratford, J. M.; Allan, P. K.; Pecher, O.; Chater, P. A.; Grey, C. P. Mechanistic Insights into Sodium Storage in Hard Carbon Anodes Using Local Structure Probes. *Chem. Commun.* **2016**, *52*, 12430–12433.
10. Stratford, J. M.; Kleppe, A. K.; Keeble, D. S.; Chater, P. A.; Meysami, S. S.; Wright, C. J.; Barker, J.; Titirici, M.-M.; Allan, P. K.; Grey, C. P. Correlating Local Structure and Sodium Storage in Hard Carbon Anodes: Insights from Pair Distribution Function Analysis and Solid-State NMR. *J. Am. Chem. Soc.* **2021**, *143*, 14274–14286.
11. Liu, M.; Zhang, J.; Guo, S.; Wang, B.; Shen, Y.; Ai, X.; Yang, H.; Qian, J. Chemically Presodiated Hard Carbon Anodes with Enhanced Initial Coulombic Efficiencies for High-Energy Sodium Ion Batteries. *ACS Appl. Mater. Interfaces* **2020**, *12*, 17620–17627.
12. Fang, H.; Gao, S.; Ren, M.; Huang, Y.; Cheng, F.; Chen, J.; Li, F. Dual-Function Presodiation with Sodium Diphenyl Ketone towards Ultra-Stable Hard Carbon Anodes for Sodium-Ion Batteries. *Angew. Chem. Int. Ed.* **2023**, *62*, e202214717.
13. Zheng, G.; Lin, Q.; Ma, J.; Zhang, J.; He, Y.-B.; Tang, X.; Kang, F.; Lv, W.; Yang, Q.-H. Ultrafast Presodiation of Graphene Anodes for High-Efficiency and High-Rate Sodium-Ion Storage. *InfoMat* **2021**, *3*, 1445–1454.
14. Park, Y.; Shin, D.-S.; Woo, S. H.; Choi, N. S.; Shin, K. H.; Oh, S. M.; Lee, K. T.; Hong, S. Y. Sodium Terephthalate as an Organic Anode Material for Sodium Ion Batteries. *Adv. Mater.* **2012**, *24*, 3562–3567.
15. Cabañero, J. M. Jr.; Pimenta, V.; Cannon, K. C.; Morris, R. E.; Armstrong, A. R. Sodium Naphthalene-2,6-Dicarboxylate: An Anode for Sodium Batteries. *ChemSusChem* **2019**, *12*, 4522–4528.
16. Desai, A. V.; Seleghini, H. S.; Rainer, D. N.; Stanzione, M. G.; Cordes, D. B.; Magdysyuk, O. V.; McKay, A. P.; Coles, S. J.; Ashbrook, S. E.; Morris, R. E.; Armstrong, A. R. Structure–Property Relationships in Disodium Anthracene Dicarboxylate for Sodium-Ion Storage via 3D Electron Diffraction. *Chem. Commun.* **2025**, *61*, 11433–11436.
17. Caroff, M.; Subash, N.; Becuwe, M.; Davoisne, C. Investigation of 2,6-Sodium Naphthalene Dicarboxylate Structure–Reactivity Relationship by Operando X-Ray Diffraction and Post-Mortem Transmission Electron Microscopy. *Chem. Mater.* **2025**, *37*, 8039–8047.
18. Deng, W.; Qian, J.; Cao, Y.; Ai, X.; Yang, H. Graphene-Wrapped $Na_2C_{12}H_6O_4$ Nanoflowers as High Performance Anodes for Sodium-Ion Batteries. *Small* **2016**, *12*, 583–587.
19. Pickard, C. J.; Needs, R. J. High-Pressure Phases of Silane. *Phys. Rev. Lett.* **2006**, *97*, 045504.
20. Pickard, C. J.; Needs, R. J. Ab Initio Random Structure Searching. *J. Phys. Condens. Matter* **2011**, *23*, 053201.
21. Wang, G.; Huang, B.; Liu, D.; Zheng, D.; Harris, J.; Xue, J.; Qu, D. Exploring Polycyclic Aromatic Hydrocarbons as an Anolyte for Nonaqueous Redox Flow Batteries. *J. Mater. Chem. A* **2018**, *6*, 13286–13293.
22. Wu, S.; Wang, W.; Li, M.; Cao, L.; Lyu, F.; Yang, M.; Wang, Z.; Shi, Y.; Nan, B.; Yu, S.; Sun, Z.; Liu, Y.; Lu, Z. Highly Durable Organic Electrode for Sodium-Ion Batteries via a Stabilized α-C Radical Intermediate. *Nat. Commun.* **2016**, *7*, 13318.
23. Tang, M.; Bui, N. N.; Zheng, J.; Song, L.; Hu, Y.-Y. Real-Time Monitoring of the Lithiation Process in Organic Electrode 7,7,8,8-Tetracyanoquinodimethane by in Situ EPR. *J. Energy Chem.* **2021**, *60*, 9–15.
24. Wang, B.; Fitzpatrick, J. R.; Brookfield, A.; Fielding, A. J.; Reynolds, E.; Entwistle, J.; Tong, J.; Spencer, B. F.; Baldock, S.; Hunter, K.; Kavanagh, C. M.; Tapia-Ruiz, N. Electron Paramagnetic Resonance as a Tool to Determine the Sodium Charge Storage Mechanism of Hard Carbon. *Nat. Commun.* **2024**, *15*, 3013.
25. Bai, Y.; Liu, T.; Peng, H.; Zhao, H.; Fan, Q.; Pan, X.; Zhou, L.; Zhao, H. Organoboron–Thiophene-Based Polymer Electrodes for High-Performance Lithium-Ion Batteries. *RSC Adv.* **2024**, *14*, 7215–7220.
26. Prill, D.; Juhás, P.; Billinge, S. J. L.; Schmidt, M. U. Towards Solution and Refinement of Organic Crystal Structures by Fitting to the Atomic Pair Distribution Function. *Acta Crystallogr. Sect. A* **2016**, *72*, 62–72.
27. Kertesz, M. Pancake Bonding: An Unusual Pi-Stacking Interaction. *Chem. – Eur. J.* **2019**, *25*, 400–416.
28. Suzuki, S.; Morita, Y.; Fukui, K.; Sato, K.; Shiomi, D.; Takui, T.; Nakasuji, K. Aromaticity on the Pancake-Bonded Dimer of Neutral Phenalenyl Radical as Studied by MS and NMR Spectroscopies and NICS Analysis. *J. Am. Chem. Soc.* **2006**, *128*, 2530–2531.
29. Cui, Z.; Lischka, H.; Beneberu, H. Z.; Kertesz, M. Double Pancake Bonds: Pushing the Limits of Strong π–π Stacking Interactions. *J. Am. Chem. Soc.* **2014**, *136*, 12958–12965.

Citation: *CCS Chem.* **2026**, Just Published. DOI: 10.31635/ccschem.026.202507155
Link to VoR: https://doi.org/10.31635/ccschem.026.202507155